

Space-Variant Polarization Patterns of Non-collinear Poincaré Superpositions

E.J. Galvez,¹ K. Beach,¹ J.J. Zeosky¹ and B. Khajavi²

¹Department of Physics and Astronomy, Colgate University, Hamilton, NY 13346, U.S.A.

²Department of Physics and Astronomy, Florida Atlantic University, Boca Raton, FL 33431, U.S.A.

ABSTRACT

We present analysis and measurements of the polarization patterns produced by non-collinear superpositions of Laguerre-Gauss spatial modes in orthogonal polarization states, which are known as Poincaré modes. Our findings agree with predictions (I. Freund *Opt. Lett.* **35**, 148-150 (2010)), that superpositions containing a C-point lead to a rotation of the polarization ellipse in 3-dimensions. Here we do imaging polarimetry of superpositions of first- and zero-order spatial modes at relative beam angles of 0–4 arcmin. We find Poincaré-type polarization patterns showing fringes in polarization orientation, but which preserve the polarization-singularity index for all three cases of C-points: lemons, stars and monstars.

Keywords: Polarization singularities, C-points, Poincaré beams

1. INTRODUCTION

Space-variant polarization is an interesting case study of complex light fields. Since eyes and cameras are oblivious to polarization, a rich aspect of light waves is largely ignored because it is unseen. Yet, extraordinary complexity is ubiquitous. Linear superposition is at the heart of this problem, as wave fields just recombine point wise to give a polarization that varies in 3 dimensions. A controlled way to study space-variant polarization is by the generation of beams are non-separable superpositions of polarization and spatial mode.¹ Research on this problem has its origins in vector beams.² Vector beams can be understood as the non-separable superposition of Laguerre-Gauss modes of the same order but with opposite topological charge and state of circular polarization. They can also be recreated with a superposition of orthogonal first-order Hermite-Gauss modes with orthogonal states of linear polarization. Both cases involve the same spatial-mode order. As a result, they form a space-variant pattern where the states of polarization vary in the angular (but not in the radial) directions in the transverse plane. By allowing modes of distinct order to form a non-separable superposition with polarization, the field that is generated has a mode where the polarization varies in the radial as well as in the angular directions, a type of mode that is known as a Poincaré, because it contains mappings of all the states represented on the Poincaré sphere.³

Previous recreations of space-variant patterns have used “designer” optical beams which are either single beams being manipulated by birefringent optical elements,^{3,4} or collinear superpositions of beams.^{1,5–10} These studies have found interesting polarization patterns in two-dimensional slices of space. The third dimension holds many more interesting patterns, as shown by research with random fields,^{11,12} as well as in the designer beams for the case of focused vector beams, where longitudinal components of the fields appear.^{13,14}

Theoretical studies of the three dimensional case of coherent light beams that are not collinear shows unique patterns.^{15–19} The most salient feature of those studies is that the polarization ellipse twists three-dimensionally in space, and when following a circular path about the axis of the beam, the polarization ellipse describes either Mobius strips or twisted ribbons. More recently, 3-dimensional polarization twists were reported in the focusing of Poincaré beams in the laboratory.²⁰

In this article we describe our attempt at understanding the problem as formulated by Freund using the interference of non-collinear Poincaré beams. In Sec. 2 we present the formalism to understand the problem, which follows that of Freund.¹⁶ In Sec. 3 we describe our apparatus, and in Sec. 4 we present our results to date.

Further author information: (Send correspondence to E.J.G.)
E.J.G.: E-mail: egalvez@colgate.edu, Telephone: 1 315 228 7205

2. THEORETICAL FRAMEWORK

The fields that we create here are in a superposition of polarization and spatial modes. In particular, the two spatial modes are in a superposition of states of circular polarization. As pointed out in more detail earlier,¹ a general form of the polarization state is given by

$$\hat{e}_{\chi,\alpha} = \cos \chi e^{i\alpha} \hat{e}_R + \sin \chi e^{-i\alpha} \hat{e}_L \quad (1)$$

represents an ellipse of ellipticity related to the relative amplitude of the two polarization components:

$$\epsilon = \frac{b}{a} = \tan^{-1} \left(\frac{\pi}{4} - \frac{\chi}{2} \right) \quad (2)$$

and an orientation equal to α , half the relative phase between the two components. Angles χ and 2α represent the polar and azimuthal angles of the Poincaré sphere.

We consider the case of component Laguerre-Gauss modes with zero radial order and topological charge ℓ . Their scalar amplitude is given by

$$LG_0^\ell = A_\ell r^{|\ell|} e^{i\ell\phi} GW, \quad (3)$$

where r and ϕ are the transverse polar coordinates; A_ℓ is the amplitude of the mode, given by

$$A_\ell = \left(\frac{2^{|\ell|+1}}{\pi |\ell|!} \right)^{\frac{1}{2}} \left(\frac{1}{w} \right)^{|\ell|+1}, \quad (4)$$

with w being the half-width of the mode; G is the gaussian function

$$G = e^{-r^2/w^2}; \quad (5)$$

and W is the wave propagator

$$W = e^{i[kz + kr^2/(2R) + \varphi]}, \quad (6)$$

where k is the wave vector, R the radius of curvature of the wavefront, and φ the Gouy phase. For our purposes we will assume that the beam has a large Rayleigh range, and so we can drop the second and third terms of Eq. 6. We also find it convenient to rework Eq. 3 as

$$LG_0^\ell = A_\ell (X + i\sigma Y)^{|\ell|} GW, \quad (7)$$

where X and Y are the transverse Cartesian components of the beam, introduced via applying the Euler identity to the azimuthal phase term of Eq. 3, and with $\sigma = \ell/|\ell|$ being the sign of the topological charge.

We interfere two beams that we know produces a recognizable C-point pattern,^{9,10} consisting of a Laguerre-Gauss mode of topological charge ℓ in one state of circular polarization with a Laguerre-Gauss of order 0 in the orthogonal state. The two beams interfere forming a relative angle 2θ , as shown in Fig. 1. The local beam coordinates of the beams, (X_ℓ, Y_ℓ, Z_ℓ) transform to the observing frame frame (x, y, z) via

$$X_\ell = x \cos \theta_\ell + z \sin \theta_\ell \quad (8)$$

$$Y_\ell = y \quad (9)$$

$$Z_\ell = x \sin \theta_\ell + z \cos \theta_\ell \quad (10)$$

Figure. 1 shows the case of two beams with topological charges ℓ and 0, and with $\theta_0 = -\theta_\ell = \theta$. The fields of the two beams in their local frames and in their circularly polarized states are:

$$\vec{E}_\ell = A_\ell (X_\ell + i\sigma Y_\ell)^{|\ell|} e^{-(X_\ell^2 + Y_\ell^2)/w^2} e^{ikZ_\ell} \left(\frac{\hat{e}_{X_\ell} - i\hat{e}_{Y_\ell}}{\sqrt{2}} \right) \quad (11)$$

$$\vec{E}_0 = A_0 e^{-(X_0^2 + Y_0^2)/w^2} e^{ikZ_0} \left(\frac{\hat{e}_{X_0} + i\hat{e}_{Y_0}}{\sqrt{2}} \right), \quad (12)$$

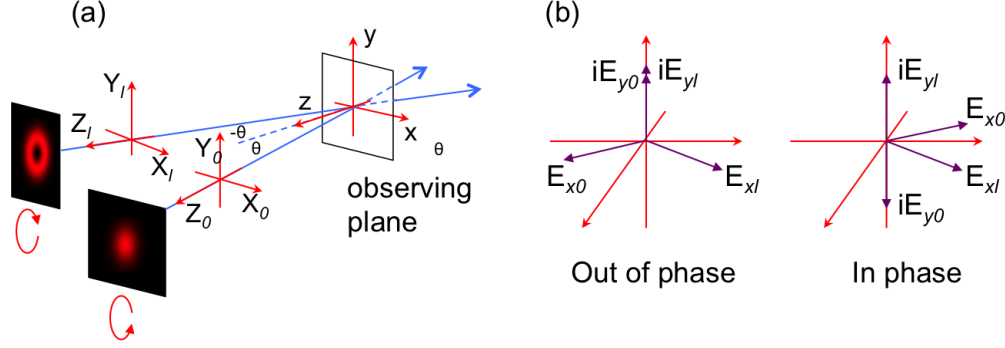


Figure 1. (a) Reference frames of the two non-collinear beams and the observing frame. (b) Orientation of the field components at points where the x -components of the fields of the two beams are out of phase and in phase.

where k is the wavenumber of the wave-field. The unit vectors also transform via

$$\hat{e}_{X_\ell} = \cos \theta_\ell \hat{e}_x - \sin \theta_\ell \hat{e}_z \quad (13)$$

$$\hat{e}_{Y_\ell} = \hat{e}_y \quad (14)$$

Below we present the results of simulations of the 3-dimensional fields using Eqs. 11 and 12.

For purposes of illustration, when $\theta_0 = -\theta_\ell = \theta$ and $z = 0$, we can write the fields in the form:

$$\vec{E}_\ell = A_\ell (x^2 \cos^2 \theta + y^2)^{|\ell|/2} e^{-(x^2 \cos^2 \theta + y^2)/w^2} e^{i[\ell \tan^{-1}(y/x \cos \theta) - kx \sin \theta]} (\cos \theta \hat{e}_x - i \hat{e}_y + \sin \theta \hat{e}_z) \quad (15)$$

$$\vec{E}_0 = A_0 e^{-(x^2 \cos^2 \theta + y^2)/w^2} e^{-ikx \sin \theta} (\cos \theta \hat{e}_x + i \hat{e}_y - \sin \theta \hat{e}_z). \quad (16)$$

It is important to highlight two features of fields in Eqs. 15 and 16. First is that because of the non-zero value of θ , the relative phase between the two component fields includes the term that depends on the transverse coordinate x , and θ , which leads to a variation in the orientation of the polarization ellipse α . When $kx \sin \theta > \pi$ we see fringes in ellipse orientation, as shown in Fig. 2. This is irrespective of the type of polarization singularity anisotropy of the pattern. The case shown corresponds to a lemon C-point. This C-point has a singularity index

$$I_C = \frac{\Delta \alpha}{2\pi} = \frac{1}{2}, \quad (17)$$

where $\Delta \alpha$ is the rotation of the polarization ellipse per closed path about the C-point. In the case shown the polarization ellipses rotate by half of a turn per closed path about the singularity. Note that regardless how wide we pick the circle about the C-point (see the case $\theta = 2.4$ arcmin in Fig. 2) the net orientation rotation remains the same, and thus conserving the value of I_C .

A second important feature of Eqs. 15 and 16 is the appearance of a z component in the fields. Fig. 3a shows gray-scaled images of the square of the three components of the field in the observing plane. Note that the fringes of the y component overlap spatially with the fringes of the z components, but are complementary to those of the x component. We can understand this with Fig. 1b: when the field components of the two beams in the x direction are in phase, due to the opposite circular polarization of the two beams, the fields in the y direction are out of phase, and because of the choice of observing plane orientation, the field components in the z direction are out of phase. The converse is true too: when the the fields in the x -direction are out of phase, the field components in the y and z directions are in phase. The images of Fig. 3a do not indicate the phase of the field. These will be important for comparing with the measurements, discussed below.

For visualizing what the total field is doing in 3 dimensions we need to construct the polarization ellipse of each point. We do this via the relations for the semi major and semi minor axes of the ellipse, given respectively

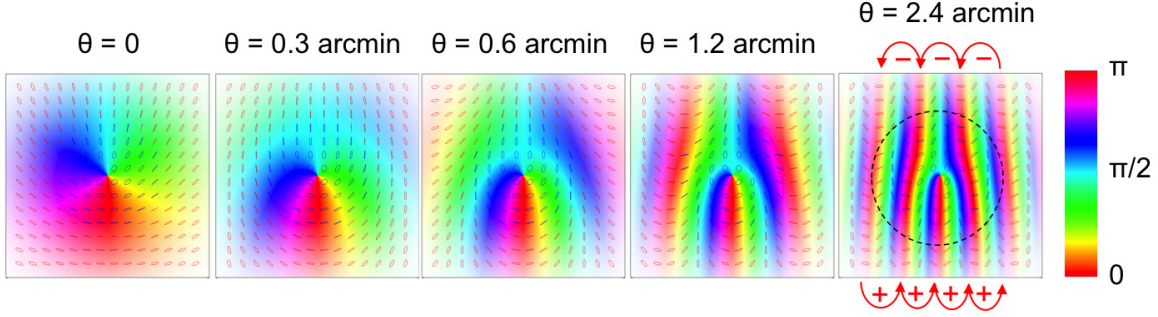


Figure 2. Projections of the polarization ellipse onto the observing plane for different values of the half-angle between the two beams θ correlated to our laboratory parameters (beam width and wavelength). The orientation of the polarization ellipses is color coded, as shown in the legend. The last pane shows the rotation of the orientation of the polarization in increments of half turns: counter clockwise (+) and clockwise (-).

by²¹

$$\bar{a} = \frac{1}{|\sqrt{\vec{E} \cdot \vec{E}}|} \text{Re} \left(\vec{E} \sqrt{\vec{E}^* \cdot \vec{E}^*} \right) \quad (18)$$

$$\bar{b} = \frac{1}{|\sqrt{\vec{E} \cdot \vec{E}}|} \text{Im} \left(\vec{E} \sqrt{\vec{E}^* \cdot \vec{E}^*} \right). \quad (19)$$

Another quantity that is useful for understanding the problem is the normal to the polarization ellipse, defined

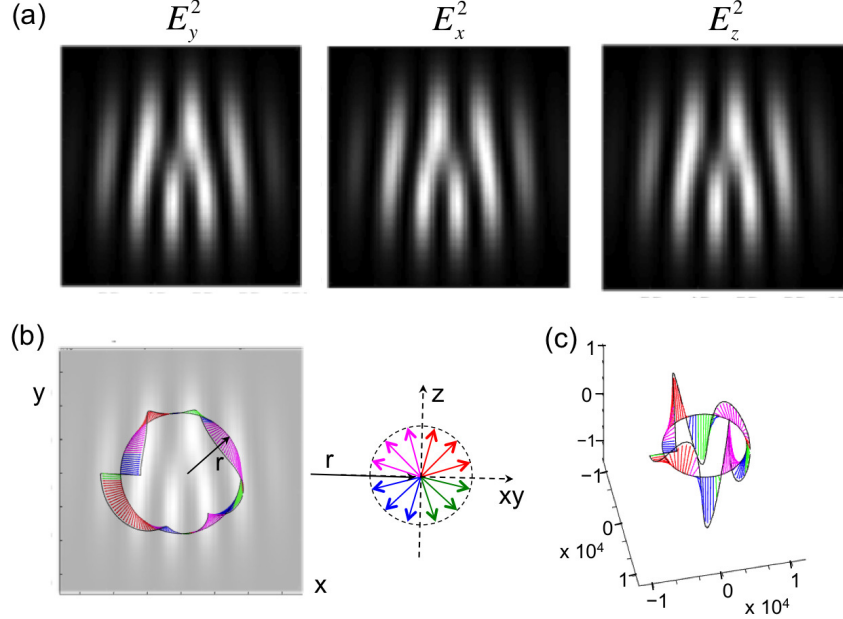


Figure 3. Analysis of the 3-dimensional character of the polarization. (a) Normalized gray scale graphs of the magnitude-squared value of the three components of the field in the observing plane. (b) Projection of the semi major axis a (with $b \sim 0$) onto the observing plane superimposed to the graph of E_z^2 . The insert to the right explains the color coding of a as described in the text and in Table 2. (c) Perspective view of the 3-dimensional vector plot of a showing how it describes a Möbius strip.

h

Table 1. Color coding of the projections of a used in Fig. 3b.

Color	$\vec{a} \cdot \hat{z}$	$\vec{a} \cdot \hat{r}$
Red	> 0	> 0
Green	< 0	> 0
Blue	< 0	< 0
Magenta	> 0	< 0
Black	$= 0$	Any

as

$$\vec{c} = \text{Im} \left(\vec{E}^* \cdot \vec{E}^* \right) = 2\vec{a} \times \vec{b} \quad (20)$$

Here we analyze the problem to the extent that is necessary to compare it with measurements. For a detailed analysis of many more aspects of the problem, see Ref. 18. Using Eqs. 18 and 19, we investigated the motion of the semi major axis in 3-dimensions along a circular path on the observing plane. This motion gives rise to a and b describing Möbius strips or twisted ribbons. That is, when we connect the ends of vectors of \vec{a} or \vec{b} along the circular path they either reconnect after an odd number of half-turns (i.e., a Möbius strip) or an integer number of full turns (twisted ribbon). The former occurs when $\ell = 1$ (lemon) or $\ell = -1$ (star). We also verified that this is the case for superpositions of $\ell = 1$ and $\ell = -1$, which give rise to monstars. It is expected that this is also the case for odd values of ℓ . Conversely, the patterns switch to twisted ribbons when ℓ is even. We have verified this for $\ell = 2$.

In Fig. 3b we show the projection of the semi major axis at a radius where the polarization is nearly linear (i.e., $b \sim 0$) for the case $\ell = 1$ and $\theta = 1.9$ arcmin (this corresponds to $r = w/\sqrt{2}$). This projection is superimposed over the fringe pattern of E_z^2 so that we can appreciate that the zero crossings of a correspond to zeros of the fringe pattern. We color code (online version) the orientation of a so that we can better appreciate its turns. This color coding is based on the projection of a onto the plane that contains the z -axis, is perpendicular to the observing plane, and which passes through the origin of a (i.e. a point on the circle). This way red corresponds to when a has components along positive- z and outward radial direction. Table 2 explains the color codings used based on the dot products of a with the unit vectors along z , \hat{z} , and along the radial direction \hat{r} . As can be seen, we see two green to red transitions and five magenta to blue transitions, for a total of 7 half turns (i.e., describing a Möbius strip). At other radii there are other odd number of half turns present: less for smaller radius and more for larger radius; the total number depends on the number of zero crossings of E_z along the circle.

The Möbius character is undoubtedly linked to the singularity index I_C . We supplement the 2-dimensional projection with a 3-dimensional view of the strip in Fig. 3c. Both confirm the claim that the polarization ellipse describes Möbius strips. We note that the scale of the z -component is 10^4 times that of the x - and y -components. This is because the angle between the two beams is very small.

3. EXPERIMENTAL METHOD

We describe here the experiments to determine the 3-dimensional character of the polarization. Because this work is ongoing, we report here only the 2-dimensional rotations of the polarization in the observing plane, and defer to a future publication the description of the measurement of the full 3-dimensional patterns.

The apparatus used for doing the experiments is similar to previous ones used in past research.¹⁰ A schematic is shown in Fig. 4. The only difference from previous works is that now the beams are not collinear. Briefly, we spatial-filter and expand a beam from a HeNe laser. It is split into two parallel components which are sent to a spatial light modulator (SLM), which diffracts the desired modes. The polarization of one of the components is rotated before the beams are recombined by a polarizing beam splitter. In this case we combine the beams in a non-collinear fashion. onto a charged-coupled-device (CCD) camera. Before the camera we placed a quarter-wave

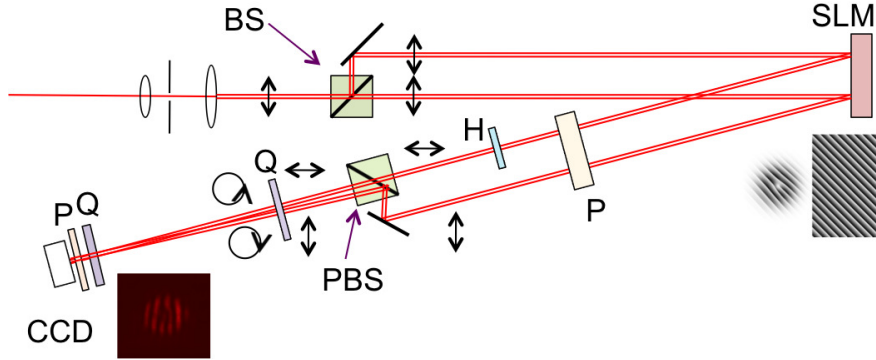


Figure 4. Apparatus used to perform the measurements. Optical components include a non-polarizing beams splitter (BS), polarizing beam splitter (PBS), half-wave plate (H), quarter-wave plates (Q), polarizers (P), and spatial light modulator (SLM). Insert shows an example the pattern encoded onto the SLM but with low fringe density for illustration purposes.

plate and a film polarizer. We used the latter to project the polarization in as close to a 2-dimensional plane as possible, given that the beams are not exactly collinear.

We used the fringe spacing recorded by the camera to extract the angle between the two beams. For the cases where the fringes were too broad, we estimated the angle from the ellipse-orientation pattern, shown below. For each case we did imaging polarimetry, recording six images past the quarter-wave plate and polarizer acting as polarization filters that transmit the linear states: horizontal, vertical, diagonal and antidiagonal; and the circular states: right- and left-handed. We then combined the images to obtain the Stokes parameters for each imaged point. We also varied the patterns displayed by the SLM to study modes with different values of ℓ and for superpositions of of the form:

$$\cos \beta LG_0^{+1} + \sin \beta e^{i\gamma} LG_0^{-1} \quad (21)$$

in one of the beams.

4. RESULTS

As mentioned earlier, here we present only partial results: the two-dimensional structure of the ellipse patterns produced by the non-collinearity of the component beams. Figure 5 shows the main results of this report. The first (a), second (b), and third (c) rows correspond respectively to $\beta = 0$ (lemon), $\beta = \pi/6$ (monstar), and $\beta = \pi/2$ (star). All three cases show fringe patterns of ellipse orientation, with false-color encoding the ellipse orientation and saturation encoding intensity. Each row represents a different angle between the component beams, denoted by the value of the half angle θ heading each column.

As the angle θ is increased one can clearly see the appearance of orientation fringes. These forked fringes are the vector counterpart of the of the phase of the scalar field that interferes with the $\ell = 0$ mode. Case (a) corresponds to fork patterns of one kind (tines pointing down), and case (c) corresponds to forks with the opposite orientation. In both cases there is a C-point at the center of the pattern. That distinction is also understood because the lemon has a singularity index $I_C = +1/2$ while the star has an index $I_C = -1/2$. They are the counterparts of optical vortices of opposite topological charge in the scalar fields. These patterns agree qualitatively with the predicted ones. Thus, they prove the first step in confirming the rotations of the polarization ellipse in 3-dimensional fields.

The case of the monstar (b) ($I_C = +1/2$) is intriguing because as the angle increases to 1 arcmin it is difficult to tell if it has a positive or negative index. The fact that the three patterns show forks with two tines indicates that they will give rise to Möbius strips.

In summary, we have studied the polarization patterns produced by non-collinear Poincaré superpositions of polarization and spatial mode. Our simulations of the problem confirm that the polarization ellipse performs

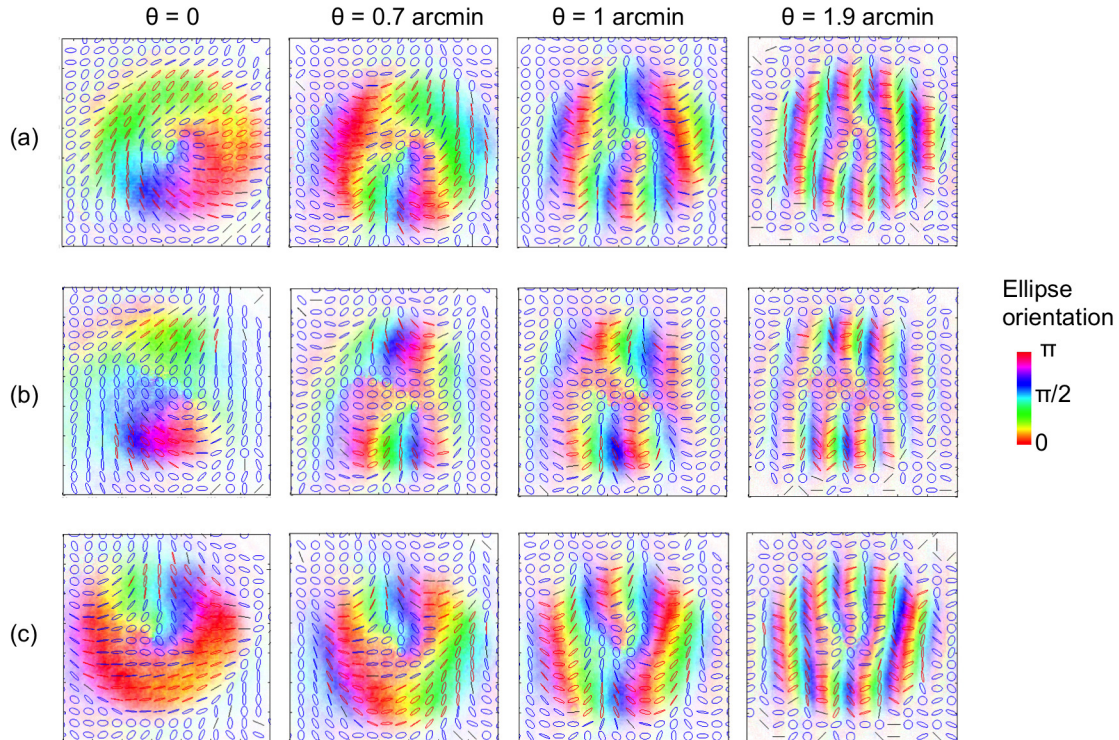


Figure 5. Measured non-collinear ellipse patterns for the case of a lemon (a), monster (b) and star (c). Color represents ellipse orientation and saturation represents intensity.

rotations of the orientation of the ellipse, giving rise to Möbius strips and twisted ribbons of the polarization along a circular path in the transverse plane. Our measurements of 2-dimensional patterns confirm the theoretical predictions. We are currently pursuing measurements of the z -component of the field that are too preliminary to present here. We expect them to be an experimental demonstration of the Möbius twists of the polarization in 3 dimensions. The results of this study only underscore the rich complexity of the general problem of light’s polarization in 3 dimensions.

5. ACKNOWLEDGMENTS

B.K. thanks W. Miller encouragement and support. This work received financial support from Florida Atlantic University and Colgate University.

REFERENCES

1. Galvez, E.J., Khadka, S., Schubert, W.H., and Nomoto, S., “Poincaré-beam patterns produced by non-separable superpositions of Laguerre-Gauss and polarization modes of light,” *Appl. Opt.* **51**, 2925–2934 (2012).
2. Zhan, Q., “Cylindrical vector beams: from mathematical concepts to applications,” *Adv. Opt. Photon.* **1**, 1–57 (2009).
3. Beckley, A.M., Brown, T.G., and Alonso, M.A., “Full Poincaré beams,” *Opt. Express* **18**, 10777–10785 (2010).
4. Cardano, F., Karimi, E., Marrucci, L., de Lisio, C., and Santamato, E., “Generation and dynamics of optical beams with polarization singularities,” *Opt. Express* **21**, 8815–8820 (2013).

5. Angelsky, O.V., Polyanskii, P.V., Mokhun, I.I., Zenkova, C.Yu., Bogatyryova, H.V., Felde, Ch.V., Bachinskiy, V.T., Boichuk T.M., and Ushenko, A.G., "Optical measurements: Polarization and coherence of light fields," in *Optical Measurements: Polarization and Coherence of Light Fields, Modern Metrology Concerns* (L. Cocco Ed.) (InTech, Rijeka, 2012) pp. 263-316.
6. Galvez, E.J., Rojec, B.L., and McCullough, K.R., "Imaging optical singularities: Understanding the duality of C-points and optical vortices," *Proc. SPIE* **8637**, 863706 1-10 (2013).
7. V. Kumar, G.M. Philip and N.K. Viswanathan, "Formation and morphological transformation singularities: Hunting the monstar," *J. Opt.* **15**, 044027 1-7 (2013).
8. Kumar, V., and Viswanathan, N.K. "Topological structures in the Poynting vector field: an experimental realization," *Opt. Lett.* **38**, 3886-3889 (2013).
9. Galvez, E.J., Rojec, B.L., and Beach K., "Mapping of all polarization-singularity C-point morphologies," *Proc. SPIE* **8999**, 89990I 1-8 (2014).
10. Galvez, E. J., Rojec, B. L., Kumar, V., and Viswanathan, N. K., "Generation of isolated asymmetric umbilicus in light's polarization," *Phys. Rev. A* **89**, 031801 (2014).
11. Flossmann, F., O'Holleran, K., Dennis, M.R., and Padgett, M.J., "Polarization Singularities in 2D and 3D Speckle Fields," *Phys. Rev. Lett.* **100**, 203902 1-4 (2008).
12. Soskin, M.S., and Vasilev, V.I., "Spacetime design of the tangled C-points and optical vortex chain and loop reactions in paraxial dynamic elliptic speckle fields," *J. Opt.* **15**, 044022 1-8 (2013).
13. Quabis, S., Dorn, R., Eberler, M., Glöckl, O., and Leuchs, G., "Focusing light to a tighter spot," *Opt. Commun.* **179**, 1-7 (2000).
14. Youngsworth, K.S., and Brown, T.G., "Focusing of high numerical aperture cylindrical vector beams," *Opt. Express* **7**, 77-87 (2000).
15. Freund, I., "Cones, spirals and Möbius strips, in elliptically polarized light," *Opt. Commun.* **249**, 7-22 (2005).
16. Freund, I., "Multitwist optical Möbius strips," *Opt. Lett.* **35**, 148-150 (2010).
17. Freund, I. "Optical Möbius strips in three-dimensional ellipse fields: I. Lines of circular polarization," *Opt. Commun.* **283**, 1-15 (2010).
18. Freund, I., "Möbius strips and twisted ribbons in intersecting Gauss Laguerre beams," *Opt. Commun.* **284**, 3816-3845 (2011).
19. Dennis, M.R., "Fermionic out-of-plane structure of polarization singularities," *Opt. Lett.* **36**, 3765-3767 (2011).
20. Bauer, T., Banzer, P., Karimi, E., Orlov, S., Rubano, A., Marrucci, L., Santamato, E., Boyd, R.W., and Leuchs, G., "Observation of optical polarization Mbius strips," *Science* 1260635 (2015).
21. Berry, M.V., "Index formulae for singular lines of polarization," *J. Opt. A* **6**, 675-678 (2004).